Constraining a simple hadronization model of relativistic heavy-ion collisions using hadronic observables

T. J. Humanic
Department of Physics, The Ohio State University, Columbus, Ohio 43210
(Received 15 July 1997)

A complicating factor in using hadrons as early probes for relativistic heavy-ion collisions is that they can undergo strong final-state rescattering with each other. This potentially causes hadronic observables to reflect the condition of the system at a late stage rather than at an early one. The present work uses a rescattering calculation with resonances to unfold these effects and thus uses measured observables to constrain a simple initial-state hadronization model for Pb+Pb collisions at CERN energies. A model parameter set is found which qualitatively agrees with measured single and two-particle observables for Pb+Pb collisions. [S0556-2813(98)05102-4]

PACS number(s): 25.75.−q, 24.10.Cn, 24.10.Lx

I. INTRODUCTION

Relativistic heavy-ion collisions provide a means of creating matter in a hot and dense state which might shed light on the behavior of matter under these extreme conditions, such as the possibility of producing a phase transition to quark matter [1]. It is generally agreed that the most extreme conditions exist in the ''initial state'' of the heavy-ion collision, roughly defined as occurring just after the projectile and target nuclei ''pass through each other.'' Eventually the interaction region hadronizes into a large number of mesons and baryons (with nonhadronic particles such as photons, electrons, and muons also being produced) and then expands to its final state. During the expansion stage the hadrons strongly scatter with each other, a process called ''rescattering.'' The final state of the collision can be thought of as the state for which rescattering ceases among all remaining (final) hadrons. It is often convenient to define the ''freeze-out'' point of a final hadron as the position, time, energy, and momentum the particle had when it stopped rescattering. Thus, one can define more precisely the final state of the collision as the collection of the freeze-out points of all of the final hadrons in an eight-dimensional phase space (four dimensions for space-time and four dimensions for momentum-energy). The term ''freeze out'' will be used to represent the final state of the collision defined in this way. In principle, the properties of the collision at freeze out are directly accessible to us by measurement. In practice, one directly measures the freeze-out momenta and energies of the particles using, for example, magnetic spectrometers [2] and indirectly measures the freeze-out space-time from the freeze-out momenta and energies using the method of two-boson interferometry [i.e., Hanbury-Brown-Twiss (HBT) interferometry] [2,3].

However, the main motivation to study relativistic heavy-ion collisions is to obtain information about the initial, extreme state of the collision. Some directly measurable nonhadronic probes such as direct photons, and electron and muon pairs have been predicted to be sensitive to certain features of the initial state and are being investigated [4]. It is equally important to study the final hadrons from the collision since they should contain information about the bulk properties of the initial state, i.e., the temperature and energy density achieved in the collision. The difficulty in using the hadrons to extract this information is that the rescattering process masks the initial space-time and momentum-energy information by random scattering and thus there is no simple connection between the freeze-out information obtained in experiments and the initial state.

In this article, the method employed to approach this problem is to use a rescattering calculation to disentangle the rescattering effects from the hadronization process. The strategy will be to take a simple model for hadronization and propagate the initial hadrons via rescattering to freeze-out, adjusting the parameters of this model to see if a parameter set can be found where the freeze-out observables from the calculation agree with those measured in experiments. Within the context of the model, this parameter set thus describes the state of the collision before rescattering, putting us a step closer in time to the initial state. The advantage of using a ''simple'' hadronization model is that the number of parameters to be adjusted is minimized, increasing the chances that the extracted parameter set is unique. The disadvantage is that some physics of the hadronization will be left out, so the physical interpretation of these parameters may be complicated. Descriptions of both the hadronization model and the rescattering calculation used are presented below. Results of applying this approach for CERN-energy Pb+Pb central collisions are then shown.

A previous paper also used a rescattering model to make predictions for CERN Pb+Pb collisions [5]. The main differences between the present calculations and those presented in Ref. [5] are summarized below.

(1) The present calculations include resonances; Ref. [5] did not. The advantage of including resonances is to make the calculations more realistic, since it is well known that resonances are present in CERN SPS (Super Proton Synchrotron)-energy collisions. Although the presence of resonances is expected to have a small effect on the radius parameters extracted from two-particle interferometry, it can have a significant effect on the intercept parameter and on the slopes of m_T distributions [6].

(2) Unlike the situation at the time of Ref. [5], preliminary

CERN Pb+Pb data are now either newly available or of higher quality than before for particle multiplicities, m_T-distribution slope parameters, rapidity distributions, and two-particle interferometry results [7–11]. This improves the input information for the calculations, and allows comparisons between the results of the calculations and data.

(3) The present space-time model for particle hadronization uses the inside-outside cascade model (IOC) [12] for the hadronization time and longitudinal position, and a projected sphere for the hadronization transverse position, similar to that used by Herrmann and Bertsch for S+Pb calculations [13]. Reference [5] used a simple ''pillbox'' geometry for the hadronization space-time. The advantage of the IOC approach is that it is Lorentz covariant. Some calculations have also been made with the pillbox geometry in the present work to compare with the IOC and with Ref. [5] (see below).

II. CALCULATIONAL METHOD

A description of the rescattering model calculational method is given below. The method used is similar to that used in previous calculations [5,14]. Rescattering is simulated with a semiclassical Monte Carlo calculation which assumes strong binary collisions between hadrons. The Monte Carlo calculation is carried out in three stages: (1) initialization and hadronization, (2) rescattering and freeze out, and (3) calculation of hadronic observables. Relativistic kinematics is used throughout. All calculations are made to simulate CERN-energy Pb+Pb collisions in order to compare with CERN experiments.

The hadronization model employs simple parametrizations to describe the initial momenta and space-time of the hadrons. The initial momenta are assumed to follow an exponential transverse momentum distribution for all particles,

$$(1/m_T)dN/dm_T = C\ \exp(-m_T/B), \tag{1}$$

where $m_T = \sqrt{(p_T^2 + m^2)}$ is the transverse mass, p_T is the transverse momentum, m is the particle mass, C is a normalization constant, and B is the slope parameter, and a Gaussian rapidity distribution for mesons,

$$dN/dy = D\ \exp[-(y-y_0)^2/(2\sigma_y{}^2)], \tag{2}$$

where $y = 0.5\ \ln[(E+p_z)/(E-p_z)]$ is the rapidity, E is the particle energy, p_z is the longitudinal momentum, D is a normalization constant, y_0 is the central rapidity value (''midrapidity''), and σ_y is the rapidity width, and a ''flat'' rapidity distribution for baryons [7]. The initial slope parameter used in Eq. (1), $B_{\rm init}$, is parametrized for each particle type as

$$B_{\rm init} = T_{\rm init} + m\beta_{\rm init}{}^2 \tag{3}$$

where $T_{\rm init}$ and $\beta_{\rm init}$ are free parameters and m is the particle mass. This parametrization has been shown to describe the mass dependence of slope parameters for freeze-out distributions of pions, kaons, and protons [8]. Its validity in the present context of hadronization slope parameters is to be determined by comparison with data (see below). The initial space-time of the hadrons is parametrized as having cylindrical symmetry with respect to the beam axis. The transverse particle density dependence is assumed to be that of a projected uniform sphere of radius equal to the projectile radius R ($R = r_0 A^{1/3}$, where $r_0 = 1.12$ fm and A is the atomic mass number of the projectile). Thus, a collision geometry with zero impact parameter is assumed. The longitudinal particle hadronization position ($z_{\rm had}$) and time ($t_{\rm had}$) are determined by the inside-outside cascade model [12]:

$$z_{\rm had} = \tau_{\rm had}\sinh(y); \quad t_{\rm had} = \tau_{\rm had}\cosh(y), \tag{4}$$

where y is the particle rapidity and $\tau_{\rm had}$ is the hadronization proper time. Thus, apart from particle multiplicities, the hadronization model has four free parameters to extract from experiment: $\sigma_{y\ \rm init}$, $T_{\rm init}$, $\beta_{\rm init}$, and $\tau_{\rm had}$.

The hadrons included in the calculation are pions, kaons, and nucleons (π, K, and N), and the ρ, ω, η, η', ϕ, Δ, and K^* resonances. For simplicity, the calculation is isospin averaged (e.g., no distinction is made between a π^+ and a π^-). However, isospin is taken into account where necessary such as in determining particle multiplicities and in properly weighting resonance production (e.g., $\pi\pi\rightarrow\rho$ is unweighted since all particles are $I=1$, but $\pi\pi\rightarrow\omega$ is weighted by $\frac{1}{3}$ since $I=0$ for the ω). Resonances are present at hadronization and also can be produced as a result of rescattering. Initial resonance multiplicity fractions are taken from Herrmann and Bertsch [13], who extract results from the HELIOS experiment [15]. The initial resonance fractions used in the present calculations are $\eta/\pi = 0.05$, $\rho/\pi = 0.1$, $\rho/\omega = 3$, $\phi/(\rho+\omega) = 0.12$, $\eta'/\eta = K^*/\omega = 1$, and, for simplicity, $\Delta/N = 0$.

The second stage in the calculation is rescattering which finishes with the freeze out and decay of all particles. Starting from the initial stage ($t = 0$ fm/c), the positions of all particles are allowed to evolve in time in small time steps ($\delta t = 0.1$ fm/c) to their initial momenta. At each time step each particle is checked to see (a) if it decays, and (b) if it is sufficiently close to another particle to scatter with it, the total elastic scattering cross section determining this ''closeness'' criterion depending on the particle types and their energies, i.e.,

$$d \leq \sqrt{(\sigma/\pi)}, \tag{5}$$

where d is the separation between the two particles and σ is the total elastic cross section. A particular particle is only allowed to scatter once with another particle in the calculation (e.g., particle No. 23 can only scatter once with particle No. 608 but both particles could then go off and scatter with other particles, etc.). Elastic scatterings between any pair of hadrons in the calculation are allowed. Isospin-averaged elastic total $\sigma(ij)$ and differential $d\sigma(ij)/d\Omega$ cross sections (where i and j symbolize particle type) were obtained for $\pi\pi$, πK, πN, and KK from Prakash *et al.* [16]. Plots of $\sigma(ij)$ versus $\sqrt{s}$ from Ref. [16] were parametrized in terms of s-wave and p-wave parameters $D^s(ij)$ and $D^p(ij)$ as

$$\sigma(ij) = D^s(ij) + D^p(ij)R(s) \tag{6}$$

and used to determine $d\sigma(ij)/d\Omega$ with

$$d\sigma(ij)/d\Omega = g[D^s(ij) + 3D^p(ij)R(s)\cos^2\theta],$$

where

TABLE I. $D^s(ij)$ and $D^p(ij)$ parameters extracted from plots from Ref. [16] using Eq. (6).

	$\pi\pi$	πK	πN	KK
D^s (fm^2)	0.8	1.0	2.0	1.0
D^p (fm^2)	1.9×10^5	1.75×10^4	3.05×10^5	0

$$R(s)=[s-(m_i-m_j)^2]/[(s-{m_r}^2)^2+{m_r}^2{\Gamma_r}^2]$$

and where s is the usual Mandelstam variable for particles i and j, m_r is the resonance mass, Γ_r the resonance width, θ the scattering angle in the $i-j$ c.m. frame, and g is a constant. Table I gives the values of D^s and D^p extracted from Ref. [16] using Eq. (6). Note that $D^s(KK)$ was assumed to be equal to $D^s(K\pi)$ and $D^p(KK)$ was assumed to be zero. For KN and NN scatterings, parametrizations for the total elastic cross sections were obtained from the Review of Particle Properties [17] and take the form

$$\sigma(ij)=a+bp^n+c(\ln(p))^2+d\ \ln(p), \tag{7}$$

where p is the momentum (in GeV/c) of one of the particles in the frame where the other particle is at rest, and a, b, n, c, and d are parameters given in Table II for KN and NN. Note that in the case of KN, $\sigma=12$ mb for $p<1$ GeV/c, and for NN, $\sigma=300$ mb for $p<0.2$ GeV/c, and $\sigma\rightarrow\sigma/2$ in Eq. (7) for $0.2<p<2$ GeV/c in order to agree with NN scattering data. As an expedient, the total elastic cross section for any case where a resonance scatters with another particle is taken to be the same as that for KK, i.e., $\sigma=10$ mb.

Resonance production is defined to always occur in a scattering event between two particles when two additional conditions are satisfied: (a) the scattering channel is correct to produce a given resonance and (b) the $\sqrt{s}$ of the scattering lies between $m_r-\Gamma_r$ and $m_r+\Gamma_r$ for that resonance. Allowed resonance production channels and their decay channels are as follows:

$$\pi\pi\rightarrow\rho\rightarrow\pi\pi,$$

$$\pi\pi\rightarrow\omega\rightarrow\pi\pi\pi,$$

$$\pi\pi\rightarrow\eta\rightarrow\pi\pi,$$

$$\pi\pi\rightarrow\eta'\rightarrow\pi\pi\pi,$$

$$\pi\pi\rightarrow\phi\rightarrow KK,$$

$$\pi N\rightarrow\Delta\rightarrow\pi N,$$

$$\pi K\rightarrow K^*\rightarrow\pi K,$$

TABLE II. Parameters of Eq. (7) for the KN and NN total elastic cross sections.

	a (mb)	b (mb)	n	c (mb)	d (mb)
$KN\rightarrow KN$	6.2	4.0	-1.8	0.23	-1.85
$NN\rightarrow NN$	11.9	26.9	-1.21	0.169	-1.85

$$KK\rightarrow\phi\rightarrow KK.$$

As already mentioned earlier, the production channels $\pi\pi\rightarrow\omega,\eta,\eta',\phi$ and $KK\rightarrow\phi$ must be weighted by $\frac{1}{3}$ to take into account isospin effects. Other possible particle production channels such as $NN\rightarrow N\Delta\rightarrow NN\pi$ and $KN\rightarrow\Lambda\rightarrow\pi N$ were not included in the present calculations for simplicity. It is felt that these omissions are at least partially justified by the fact that the π, K, and N multiplicities resulting from the rescattering calculation are forced to agree with experiment and thus these channels cannot effect the final particle multiplicities. However, leaving out these channels could have more subtle effects, for example, on the shapes of the K and N transverse momentum distributions. Clearly, this is neither a perfect nor complete implementation of resonances. It is meant to take into account the gross features of resonances in the spirit of the present simple rescattering model.

Once it is determined that the particle pair is close enough to scatter from Eq. (5), the scattering is then carried out using relativistic kinematics to determine the scattered momenta of the two particles. A ''scattering time'' of 0.2 fm/c is imposed on the interaction such that neither particle is allowed to scatter again with another particle during this time period. Each particle is followed in time until its last scattering (i.e., freeze out) or, if it is a resonance, until it decays after freeze out at which point its space-time position and momentum are recorded. For the Pb+Pb collisions considered in the present calculation, particles undergo about fifteen scatterings on average before freeze out.

Calculations are carried out assuming initial parameter values and particle multiplicities for each type of particle. In the last stage of the calculation, the freeze-out and decay momenta and space-times are used to produce single-particle and two-particle observables such as pion, kaon, and nucleon multiplicities, transverse momentum and rapidity distributions, and two-boson correlation functions. The values of the initial parameters of the calculation are constrained to give observables which agree with available measured hadronic observables. For the Pb+Pb calculations studied in the present work, measured observables were obtained from the NA44 [8,9] and NA49 [7,10,11] experiments, both of which studied Pb+Pb collisions for incident kinetic energies of $E_{\rm lab}=158$ GeV/nucleon.

For the two-particle correlation calculations, the two-boson correlation function is formed and a Gaussian model for the boson source distribution is fitted to it to extract the final radius parameters. In the present calculation boson statistics are introduced using a method of pair-wise symmetrization of bosons in a plane-wave approximation [18]. The final step in the calculation is extracting radius parameters by fitting a parametrization to the Monte Carlo produced two-boson correlation function $C(Q)$, where Q is the four-vector difference between the momenta of the two bosons, i.e., $Q=p_1-p_2$. The usual parametrization of $C(Q)$ is obtained by assuming a Gaussian space-time distribution of freeze-out points, $\rho(\mathbf{r},t)$ in terms of the transverse-plane variables $r_{T\ \rm side}$ and $r_{T\ \rm out}$, the longitudinal variable along the beam direction z, and time t:

$$\rho(\mathbf{r},t)=F\ \exp(-{r_{T\ \rm side}}^2/2{\mathcal{R}_{T\ \rm side}}^2-{r_{T\ \rm out}}^2/2{\mathcal{R}_{T\ \rm out}}^2$$

TABLE III. Initial particle multiplicities used in the rescattering calculation.

π	K	N	ρ	ω	η	η'	K^*	ϕ
1010	65	534	184	61	46	46	61	29

$$-z^2/2\mathcal{R}_{\text{long}}{}^2-t^2/2\tau^2), \tag{8}$$

where $\mathcal{R}_{T\ \text{side}}$ is a transverse sideward radius parameter, $\mathcal{R}_{T\ \text{out}}$ is a transverse outward radius parameter, $\mathcal{R}_{\text{long}}$ is a longitudinal radius parameter, τ is a lifetime parameter, and F is a normalization constant [2]. From this distribution function the following parametrization of $C(Q)$ can be obtained [19]:

$$C(Q_{T\ \text{side}},Q_{T\ \text{out}},Q_{\text{long}})=G[1+\lambda\ \exp(-Q_{T\ \text{side}}{}^2R_{T\ \text{side}}{}^2 - Q_{T\ \text{out}}{}^2R_{T\ \text{out}}{}^2-Q_{\text{long}}{}^2R_{\text{long}}{}^2)], \tag{9}$$

where Q has been broken up into the two transverse and longitudinal components, G is a normalization constant, and λ is the usual empirical parameter added to help in the fitting of Eq. (9) to the ''actual'' correlation function ($\lambda=1$ in the ideal case). The radius parameters in Eq. (9) are related to those in Eq. (8) in, for example, the LCMS frame (longitudinally comoving system in which the longitudinal boson pair momentum vanishes) as follows [20]:

$$R_{T\ \text{side}}{}^2=\mathcal{R}_{T\ \text{side}}{}^2;\quad R_{T\ \text{out}}{}^2=\mathcal{R}_{T\ \text{out}}{}^2+\beta_T{}^2\tau^2;$$

$$R_{\text{long}}{}^2=\mathcal{R}_{\text{long}}{}^2,$$

where β_T is the transverse velocity of the boson pair. Note that Eq. (9) follows from Eq. (8) under the assumption of a geometrically static boson source. In a realistic heavy-ion collision the source will not be static and may have position-momentum correlations and other effects that could make the source parameters defined above depend on the boson pair momentum [21]. In the present application, Eq. (9) is fitted to the correlation function generated by the rescattering calculation as described above to extract the radius parameters $R_{T\ \text{side}}$, $R_{T\ \text{out}}$, and R_{long}.

III. RESULTS AND DISCUSSION

Results of rescattering calculations for central CERN-energy Pb+Pb collisions are presented below. Centrality in these calculations is determined by both the zero-impact-parameter assumption for the initial geometry discussed above and the preliminary NA49 particle multiplicities used which were measured with a central collision trigger [7]. Based on the measured NA49 multiplicities, the final (isospin integrated) π, K, and N multiplicities taken for the rescattering calculations were 1836, 184, and 534, respectively. Using these multiplicities and the resonance fractions given earlier, the initial particle multiplicities are uniquely determined and are given in Table III. Table IV gives the hadronization model parameters $\sigma_{y\ \text{init}}$, T_{init}, β_{init}, and τ_{had}, which are favored when comparisons are made between the rescattering calculation rapidity distributions, m_T distributions, and pion interferometry results and experimental data. The sensitivity of the hadronic observables to these parameters is discussed later. Unless otherwise noted, the rescattering model results shown below were obtained with the parameter set in Table IV. With these initial parameters defined, it is possible to calculate the total energy of the system by summing over the energies of all hadrons and thus calculate the equivalent lab bombarding energy for a Pb projectile in the model. The result of this calculation gives an equivalent beam energy of 185 GeV/nucleon, which is 17% higher than the CERN Pb-beam energy of 158 GeV/nucleon. This small difference in beam energy is not expected to effect the comparison between calculation and experiment significantly. In order to see how well the present rescattering calculation conserves energy, the total energy of the system is calculated at each time step during the full time range of the rescattering calculation. The variation in the total c.m. energy of the system is found to be about ± 11 MeV out of 3890 GeV or about $\pm 0.00028\%$.

TABLE IV. Hadronization model parameters used in the rescattering calculation which are favored by experimental data.

τ_{had} (fm/c)	T_{init} (MeV)	β_{init}	$\sigma_{y\ \text{init}}$
1	270	0.0	1.2

Figure 1 shows a plot of the average number of scatterings per time experienced by each particle in an event versus elapsed time. As is true for all such elapsed-time plots shown below, the time axis refers to times after the hadronization proper time, i.e., t-τ_{had}. As expected, the maximum scattering rate of 0.35 scatterings/(fm/c) occurs for the earliest times when the particle density is highest and rapidly falls off at later times as the system expands.

Figures 2, 3, and 4 show rescattering model plots representative of the space-time geometry of the pions, kaons, and nucleons after freeze-out (and resonance decay) for particles at midrapidity ($-1<y<1$) and a p_T range of $p_T<1$ GeV/c. For comparison, plots are also shown where rescattering has been turned off in the calculation to gauge how large the rescattering effect is. Note that for these figures the vertical axis is always plotted on a log scale and the relative normalizations for the different particles are main-

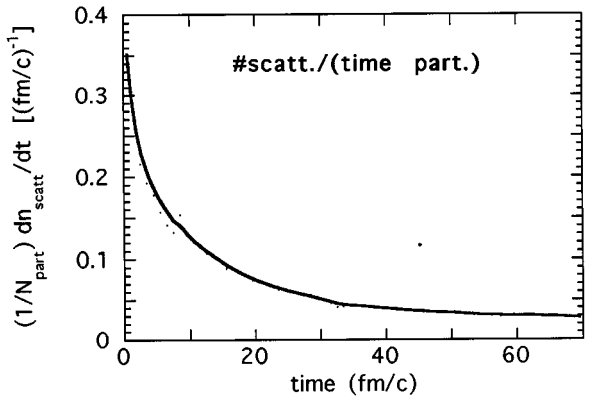

FIG. 1. Average number of scatterings per time experienced by each particle in an event versus elapsed time.

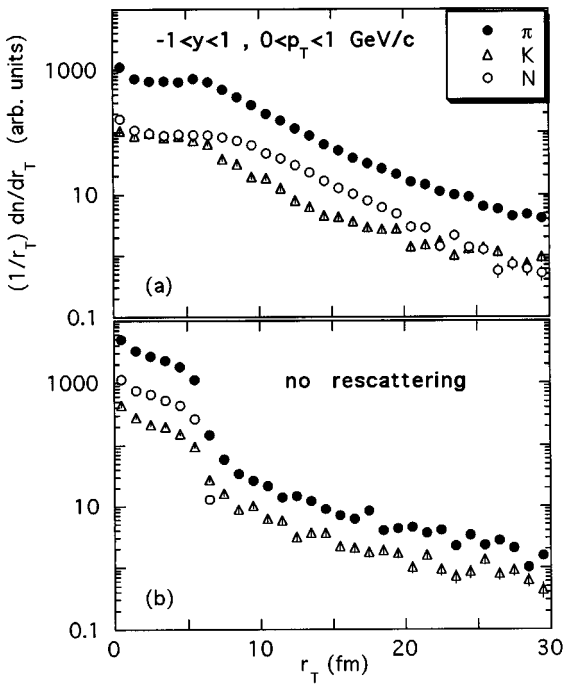

FIG. 2. Transverse radius distribution of pions, kaons, and nucleons at freeze-out (and decay) (a) from a full rescattering calculation, and (b) with rescattering turned off in the calculation. Relative normalizations are correct.

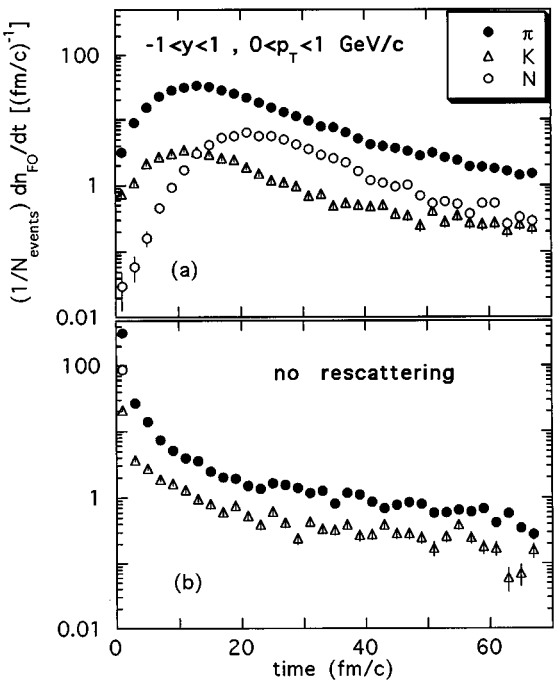

FIG. 4. Freeze-out (and decay) time distributions for pions, kaons, and nucleons (a) from a full rescattering calculation, and (b) with rescattering turned off.

tained. Figure 2 shows the transverse radius distribution. With rescattering the distribution is approximately flat up to about 6 fm (the radius of Pb is 6.64 fm) and then exponentially falls off with increasing radius for each particle type. With rescattering turned off, the projected spherical distribution of the initial state is clearly seen up to the Pb radius and then a sharp drop-off is seen followed by an exponentially decreasing dependence for pions and kaons which is due to resonance decays. Figure 3 shows the position distribution along the beam direction (z coordinate). In the rescattering case, the particles are spread out over a wide range of z, whereas without rescattering particles are sharply peaked at $z=0$ fm, the tails to higher z for pions and kaons occurring due to resonance decay. Figure 4 shows the freeze-out (and decay) time distributions for final particles. With rescattering, the distributions are peaked at different freeze-out times, the peak for kaons occurring earliest (at about 10 fm/c) and the peak for nucleons occurring latest (at about 21 fm/c), the pion peak being slightly later than for kaons (about 12 fm/c). Without rescattering the only feature to be seen is the exponential decay of the initial resonances producing pions and kaons. One can thus conclude from these figures that rescattering has a dramatic effect on the space-time of the particles in the collisions.

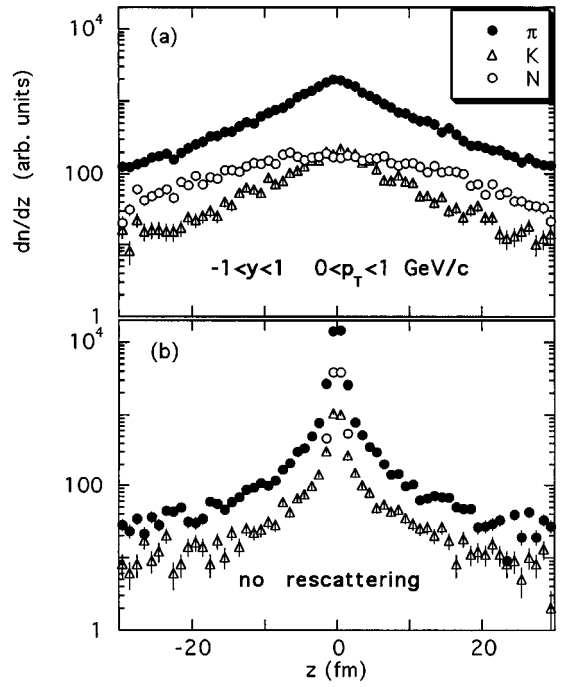

FIG. 3. Longitudinal coordinate distributions of pions, kaons, and nucleons. See Fig. 2 caption.

Figures 5, 6, and 7 show rescattering model plots representative of the momenta of the pions, kaons, and nucleons after freeze-out (and resonance decay). Figure 5 shows rapidity distributions for pions, kaons, and nucleons in the initial NN-collision c.m. frame. The pion and kaon distributions appear Gaussian shaped with $\sigma_y=1.48$ and 1.37, respectively, when Eq. (2) is fitted to them. These freeze-out widths are greater than the initial width of $\sigma_{y\ \mathrm{init}}=1.2$ assumed for the meson hadronization rapidity distributions, and are consistent with the pion and kaon widths measured by NA49 [7]. The nucleon distribution is essentially unchanged from the ''flat'' initial distribution put in before rescattering (although with some structure on the ''flat-top'') falling off sharply for $|y|>2$ as is the case for the measured ''proton'' rapidity distribution (positive hadrons minus negative hadrons) from NA49 [7]. Figure 6 shows m_T distributions for midrapidity

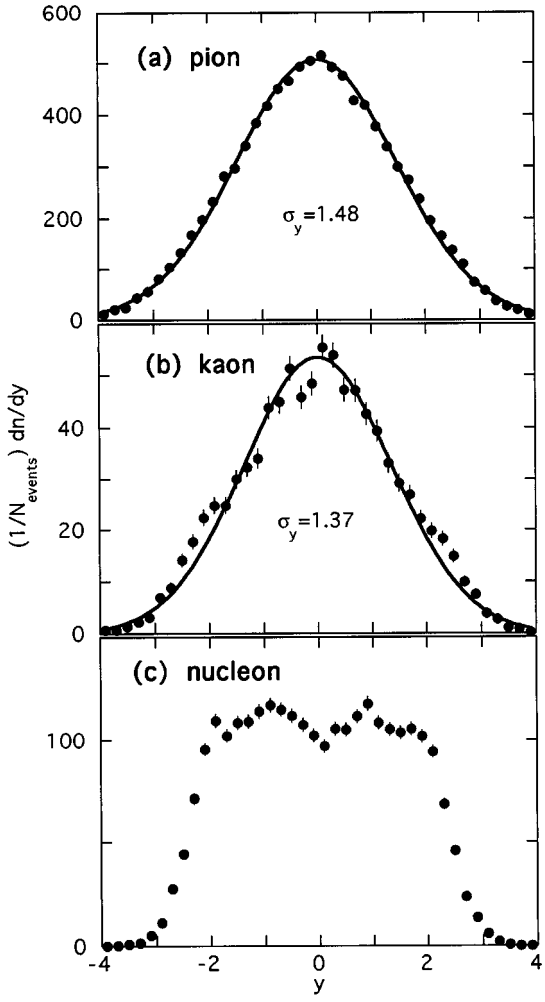

FIG. 5. Freeze-out rapidity distributions for (a) pions, (b) kaons, and (c) nucleons from the rescattering calculation. Fits to Eq. (2) for pions and kaons are also shown.

$(-1<y<1)$ pions, kaons, and nucleons at freeze-out (arbitrary normalizations) along with fits of Eq. (1). The extracted slope parameters [B in Eq. (1)] of 161, 204, and 307 MeV for pions, kaons, and nucleons, respectively, are close to the recently published Pb+Pb slope parameters from NA44 [8].

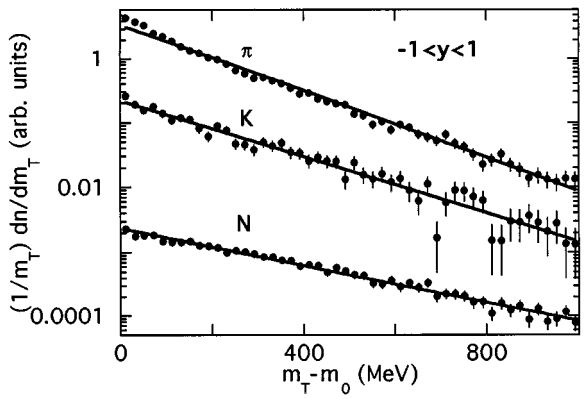

FIG. 6. m_T distributions at freeze-out from the rescattering calculation for pions, kaons, and nucleons at midrapidity. Normalizations are arbitrary. Fits to Eq. (1) are also shown.

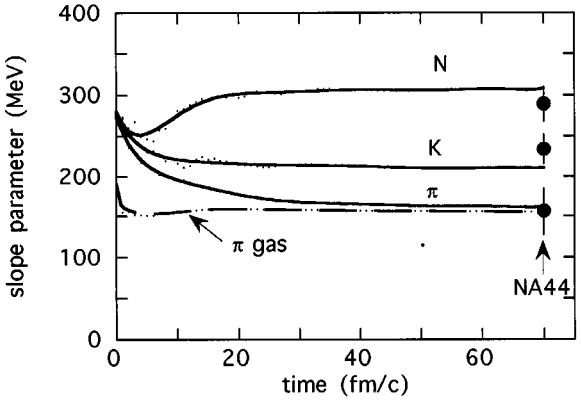

FIG. 7. Time evolution of the slope parameters in the rescattering calculation for a full calculation (solid lines) and for a ''pion gas'' calculation (dashed line). Experimental freeze-out slope parameters from NA44 (points) are plotted for comparison at 70 fm/c.

Figure 7 shows the time evolution of the slope parameters in the rescattering calculation along with a comparison with the measured NA44 values plotted near freeze-out at 70 fm/c (note that systematic errors are included in the NA44 error bars). As seen, the slope parameters evolve from the common initial value of 270 MeV into the different values of slope parameters at freeze out such that $B_\pi<B_K<B_N$. For early times (<5 fm/c) the slope parameters for all three particle types rapidly decrease with time (analogous to the adiabatic expansion experienced by opening a compressed-gas bottle and having ice forming on the valve) after which the pions and kaons continue to decrease until about 30 fm/c when their slope parameters remain essentially constant in time (analogous to the isothermal expansion stage of a freely expanding gas). This is consistent with the rapid initial decrease of rescattering followed by a slow decrease as already seen in Fig. 1. After the initial rapid decrease in B, the nucleon slope parameter increases in time until it also becomes essentially constant after about 20 fm/c, having a value almost the same as but slightly higher than the initial slope parameter of the system. This subsequent increase in the nucleon slope parameter can be explained by the large scattering cross sections for πN and, of lesser importance, KN and simple kinematics. Since the nucleon is more massive than either the pion or kaon, whenever such a scattering takes place there is a net momentum transfer to the nucleon (the lighter particle recoils in a frame initially at rest with the nucleon), reflected in the increase of the nucleon slope parameter and decrease in the pion (or kaon) slope parameter. This sort of argument also explains why the kaon slope parameter at freeze-out is larger than the pion slope parameter, since in πK scattering there is a net momentum transfer to the more massive kaon. For comparison, also plotted in Fig. 7 is a rescattering calculation for a ''pion gas'' where only π, ρ, ω, η, and η' are present and $T_{\rm init}$ is set to 190 MeV in order for the pion slope parameter to agree with NA44 at freeze out. Two interesting features are noticed in the ''pion gas'' case: (1) the initial slope parameter must be set much lower in the ''pion gas'' case than in the case where all particles are present, showing the significant influence that including the nucleons (and to lesser extent, kaons) has on the initial transverse momenta in the calculation, and (2) the

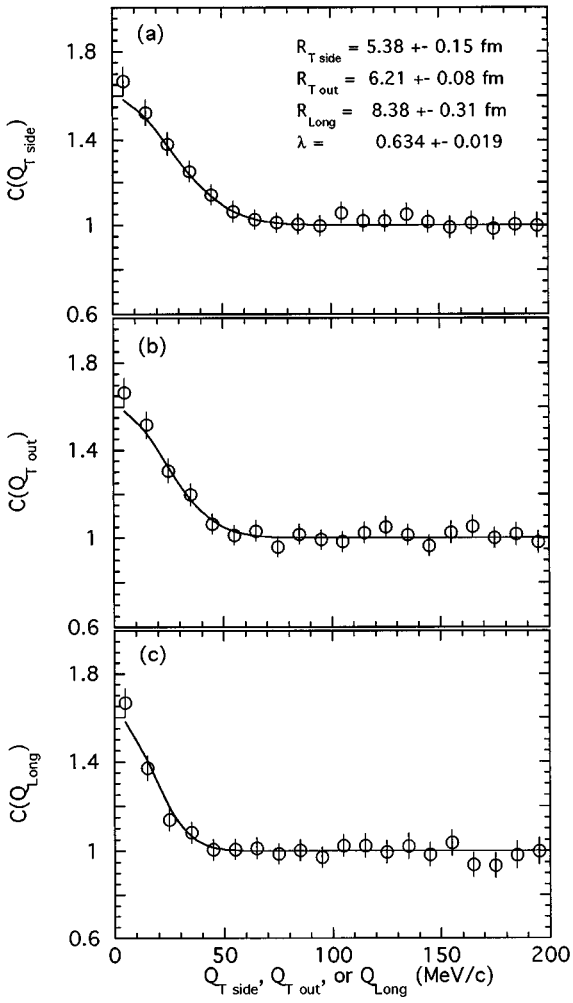

FIG. 8. Projections of the three-dimensional two-pion correlation function $C(Q_{T\ \mathrm{side}}, Q_{T\ \mathrm{out}}, Q_{\mathrm{long}})$ onto the $Q_{T\ \mathrm{side}}$, $Q_{T\ \mathrm{out}}$, and Q_{long} axes where cuts on the other two axes of $Q_j < 10$ MeV/c, $Q_k < 10$ MeV/c have been made. A fit with Eq. (9) has also been superimposed onto the Monte Carlo points.

''pion gas'' slope parameter becomes essentially constant in time immediately after a very sharp initial decrease, i.e., after 3 fm/c. The main mechanism causing the initial sharp transverse momentum drop in the ''pion gas'' as well as in the full calculation with all particles is the transfer of transverse momentum into the longitudinal component via rescattering (note that the width of the rapidity distribution for pions in the ''pion gas'' case is $\sigma_y = 1.45$, almost exactly the same as for the pion rapidity distribution in Fig. 5). This explanation is consistent with the observations made above that the freeze-out rapidity widths in Fig. 5 for pions and kaons increase whereas the nucleon rapidity distribution is essentially unchanged compared with the initial distributions, since the pion and kaon slope parameters decrease and the nucleon slope parameter remains almost the same at freeze-out.

Figures 8–12 show rescattering model results where the methods described in the previous section have been applied to extract two-boson interferometry source parameters. Figure 8 shows projections of the three-dimensional two-pion correlation function $C(Q_{T\ \mathrm{side}}, Q_{T\ \mathrm{out}}, Q_{\mathrm{long}})$ onto the $Q_{T\ \mathrm{side}}$, $Q_{T\ \mathrm{out}}$, and Q_{long} axes where cuts on the other two axes of $Q_j < 10$ MeV/c, $Q_k < 10$ MeV/c have been made. A

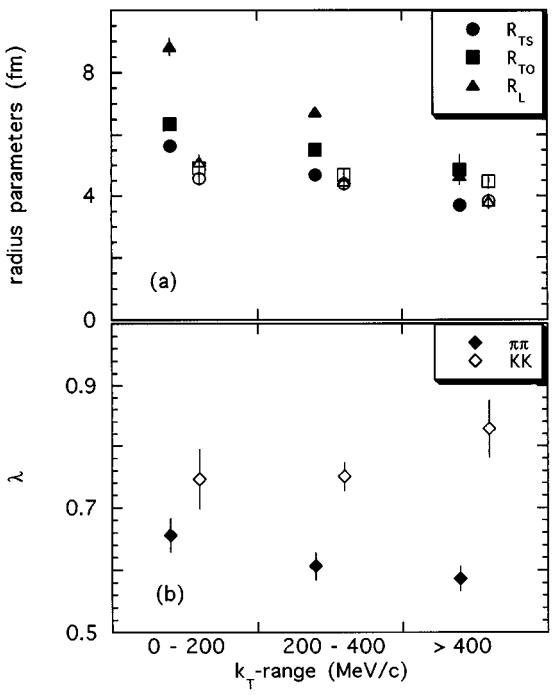

FIG. 9. k_T dependences of pion (solid symbols) and kaon (open symbols) (a) radius and (b) λ parameters extracted at midrapidity $(-1 < y < 1)$ from the present rescattering calculation.

fit with Eq. (9) has also been superimposed onto the Monte Carlo points, the extracted pion source parameters being displayed in the figure. The pion acceptance used for the calculation of this correlation function was $-1 < y < 1$ and $p_T < 400$ MeV/c, leading to an average k_T ($k_T = |\mathbf{p}_{T_1} + \mathbf{p}_{T_2}|/2$) of about 140 MeV/$c$. The main difference between these source parameters and ones extracted from rescattering calculations without resonances [5] is seen in the λ parameter: without resonances $\lambda \approx 1$ and with resonances $\lambda < 1$, in this case about 0.6. As has been pointed out previously [6], this reduction in λ is mainly due to the presence of long-lived resonances (e.g., η and η'). Figure 9 shows the k_T depen-

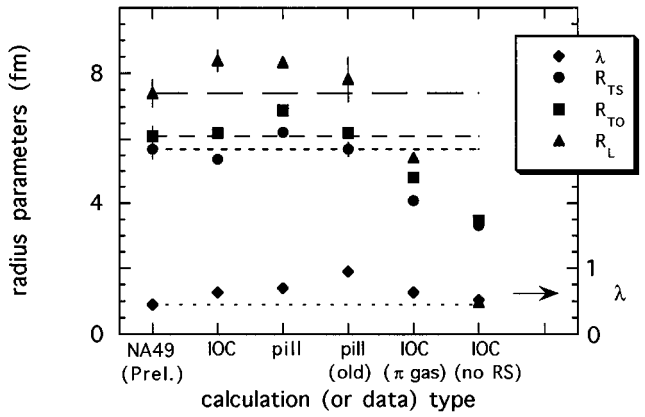

FIG. 10. Comparison between preliminary NA49 experimental pion interferometry results for Pb+Pb for the same average k_T and y range as used in Fig. 8 [10,11] and various rescattering model calculations. The dashed lines are projections of the experimental data points to allow an easier comparison with the calculations.

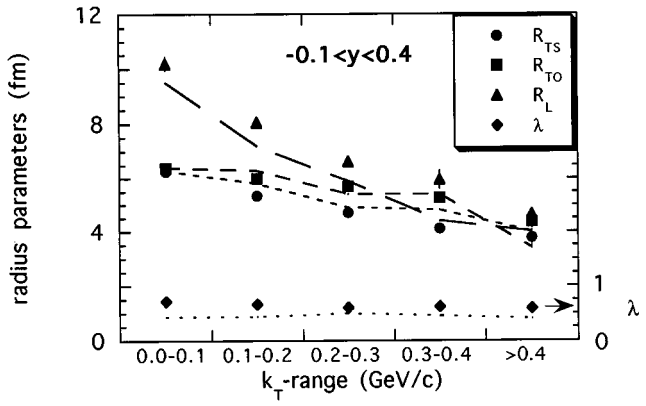

FIG. 11. Comparisons between calculations and NA49 measurements of the k_T dependence of the pion source parameters. The trends of the NA49 measurements are indicated by the dashed lines, which have similar identifications as in Fig. 10.

dences of pion and kaon source parameters extracted at midrapidity ($-1<y<1$) from the present rescattering calculation for central Pb+Pb collisions. Looking at the radius parameters first, there is a general trend for these parameters to decrease with increasing average k_T which is rather strong in the case of pions and weaker for kaons. Comparing the pion and kaon radius parameters at low k_T, the most striking difference seen between them is $R_{\rm long}$ is significantly larger than $R_{T\ \rm side}$ and $R_{T\ \rm out}$ for pions but for kaons all radius parameters are about equal. This feature is also seen in preliminary boson interferometry data from NA44 [9]. The k_T dependences of the pion and kaon λ parameters is seen to be weak in Fig. 9, but appear to go in opposite directions for pions (decreasing λ for increasing k_T) and kaons (increasing λ for increasing k_T). This could perhaps be due to the different resonances that contribute to pion production (ρ, ω, η, η', Δ) and kaon production (ϕ). Figure 10 presents a quantitative comparison between preliminary NA49 experimental pion interferometry results for Pb+Pb [10,11] for the same average k_T and y range as used in Fig. 8 and various rescattering model calculations. Note that the preliminary NA49

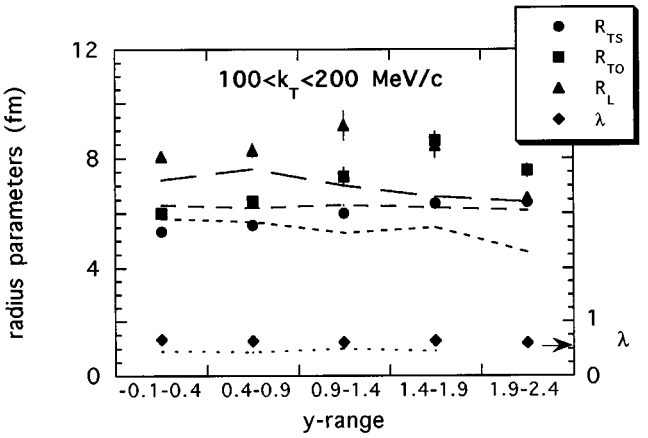

FIG. 12. Comparisons between calculations and NA49 measurements of the y dependence of the pion source parameters. The trends of the NA49 measurements are indicated by the dashed lines, which have similar identifications as in Fig. 10.

interferometry results are from charged hadron pairs since particles are not identified in this data set. Since pions largely dominate the hadron multiplicity, it should be a good approximation to consider these ''pion pairs.'' The NA49 results shown in the present paper are averaged over h^+h^+ and h^-h^-. The dashed lines are simply projections of the experimental data points to allow an easier comparison with the calculations. The five rescattering model calculations for which results are shown in Fig. 10 are the following: (1) IOC—this is the full calculation from the present work, results of which are shown in Fig. 8, (2) pill—this is a rescattering calculation with resonances from the present work, where instead of using the IOC+projected sphere initial space-time model, a uniformly distributed pillbox of 2×1 fm thickness of the type used in the previous work [5] is used, (3) pill (old)—pillbox rescattering calculation without resonances and carried out with estimated particle multiplicities from the previous work [5], (4) IOC (π gas)—rescattering calculation from the present work where only π, ρ, ω, η, and η' are present as described above in relation to Fig. 7, and (5) IOC (no RS)—calculation from the present work where rescattering is turned off but resonances are still present as described above in relation to Figs. 2, 3, and 4. Comparing the NA49 results with calculations (1), (2), and (3), all three calculations show qualitative agreement with experiment, although for (3) the λ parameter is understandably too high since no resonances are present. For the ''pion gas'' calculation (4), the radius parameters are seen to be significantly lower than experiment and calculation (1) where kaons and nucleons (and their associated resonances) are included, showing that these additional particles are necessary in order to explain the data. Finally, comparing calculation (5), the no-rescattering case, with experiment demonstrates as was already seen in Figs. 2, 3, and 4 that rescattering has a qualitatively large effect on the space-time of the hadrons emitted in Pb+Pb collisions and thus the combination of the initial radius of the Pb and resonance decay is far from sufficient to explain the large experimental radius parameters. Figures 11 and 12 show direct comparisons between calculations and NA49 measurements [10,11] of the k_T and y dependences of the pion source parameters. The trends of the NA49 measurements are indicated by the dashed lines. The pion source parameters from the present rescattering calculations are seen to qualitatively follow the trends in the preliminary NA49 pion interferometry measurements.

All of the results shown above for full IOC calculations, i.e., with all particles included, with rescattering, and including resonances (e.g., the rescattering calculation carried out for Fig. 8), have used the initial hadronization model parameters shown in Table IV. Although calculations based on this parameter set have been seen above to qualitatively agree with experimental results, this does not imply that the parameter set in Table IV is unique. Since the ultimate goal of the present study is to have extracted some information about the state of the collision around the time of hadronization, or in terms of the present simple calculation obtain a unique parameter set for the hadronization model, it is important to study how sensitive the hadronic observables are to these parameters. In the study presented below, it is found that $T_{\rm init}$ and $\beta_{\rm init}$ depend on the parameter $\tau_{\rm had}$, although $\sigma_{y\ \rm init}$ is

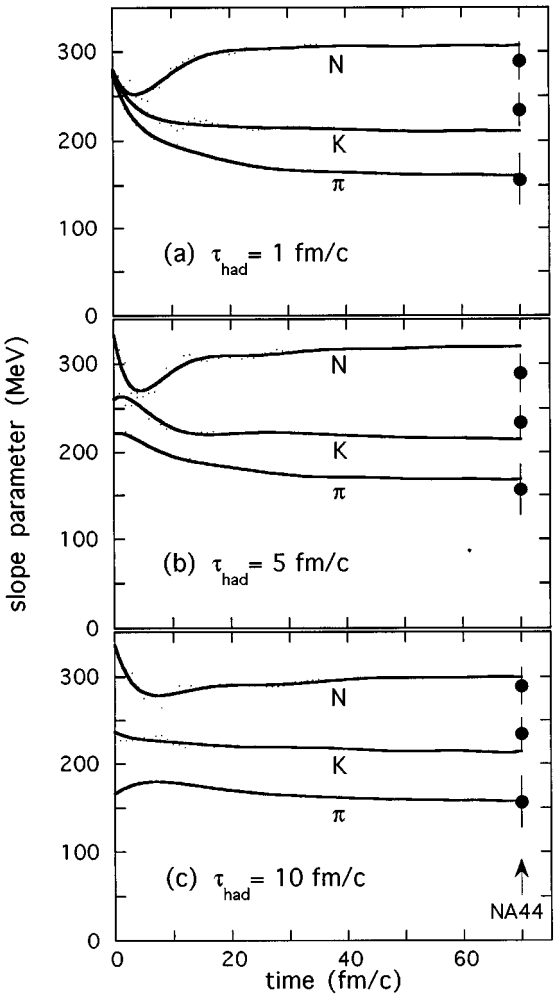

FIG. 13. Time evolution for Pb+Pb collisions of pion, kaon, and nucleon slope parameters [see Eq. (1)] calculated for midrapidity particles for three different values of $\tau_{\rm had}$ [see Eq. (4)]: (a) 1 fm/c, (b) 5 fm/c, and (c) 10 fm/c. For comparison, pion, kaon, and proton slope parameters from experiment NA44 are also shown (error bars are statistical+systematic).

fairly insensitive to $\tau_{\rm had}$. Thus it is possible to set $\sigma_{y\ \rm init}$ to its value in Table IV and concentrate on the parameters $\tau_{\rm had}$, $T_{\rm init}$, and $\beta_{\rm init}$.

Figures 13–16 show results of the study of the sensitivity of the hadronic observables on $\tau_{\rm had}$, $T_{\rm init}$, and $\beta_{\rm init}$. Figure 13 shows the time evolution of midrapidity slope parameters, as in Fig. 7, for pions, kaons, and nucleons for three different hadronization proper times [defined in Eq. (4)], i.e., $\tau_{\rm had}$=1, 5, and 10 fm/c. As in Fig. 7, the calculated asymptotic values are compared with pion, kaon, and proton slope parameters measured by the NA44 experiment (dots) [9]. As seen, reasonably good agreement can be obtained with experiment for each $\tau_{\rm had}$ as long as the initial slope parameters are chosen appropriately, i.e., $T_{\rm init}$ and $\beta_{\rm init}$ in Eq. (3) are chosen appropriately. It should be noted that a slightly better match between the calculated and experimental slope parameters could be obtained by varying the initial slope parameters individually for each particle type in the calculation. However, using Eq. (3) is considered to be a better method since $B_{\rm init}$ for all particle types is conveniently parametrized in terms of only two parameters, i.e., $T_{\rm init}$ and $\beta_{\rm init}$. Figure

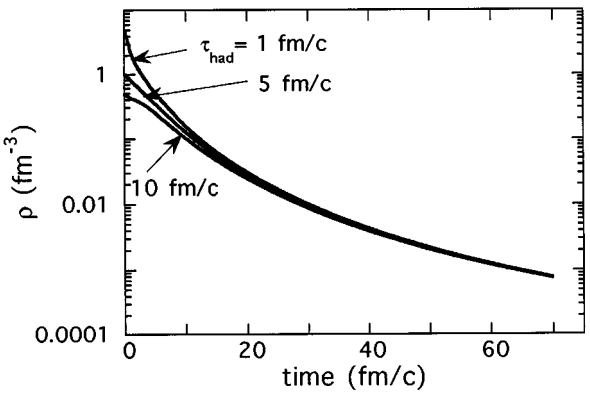

FIG. 14. Time evolution of the total particle density in Pb+Pb collisions for the three different values of $\tau_{\rm had}$.

13(a), which shows the $\tau_{\rm had}$=1 fm/c case, is identical to Fig. 7. As discussed above, this case is particularly interesting since $\beta_{\rm init}$=0 and thus $B_{\rm init}$=$T_{\rm init}$=270 MeV for all particles so that the differences in the freeze-out slope parameters for different particle types is completely due to rescattering ef-

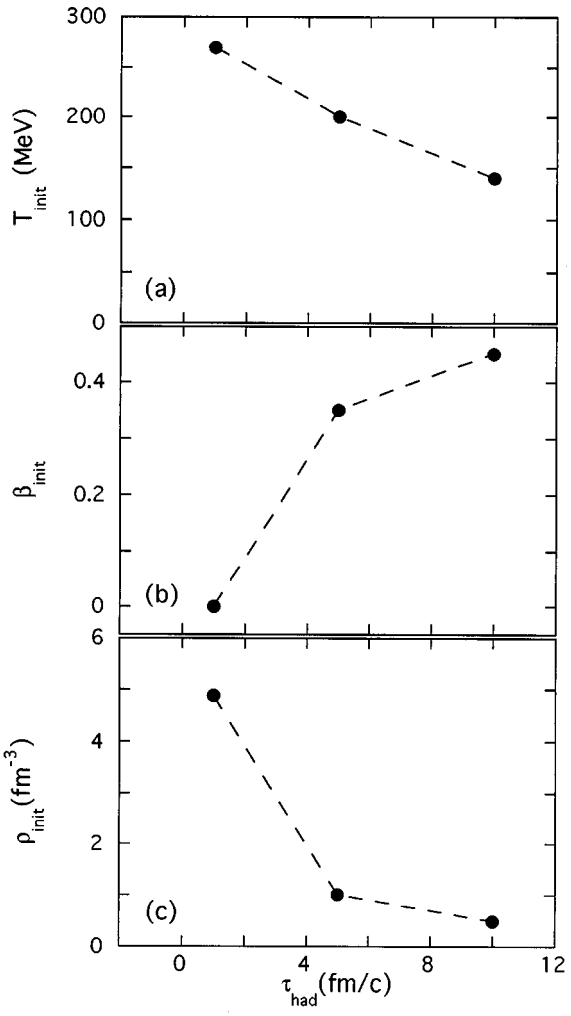

FIG. 15. Dependence of (a) $T_{\rm init}$, (b) $\beta_{\rm init}$, and (c) $\rho_{\rm init}$ on the hadronization proper time $\tau_{\rm had}$. Calculations were made for $\tau_{\rm had}$ =1, 5, and 10 fm/c (dots). The dashed lines are to guide the eye.

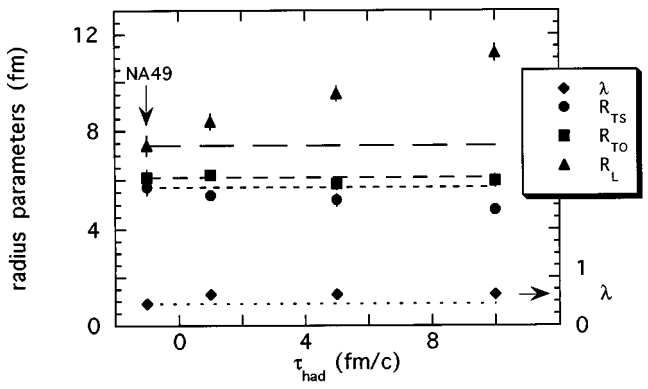

FIG. 16. Dependence of HBT-extracted two-boson source parameters on $\tau_{\rm had}$ for pion pairs. Comparison is made with preliminary NA49 pion interferometry results as in Fig. 10.

fects. In Fig. 13(b), $\tau_{\rm had}=5$ fm/c and hadronization is more spread out in time and along z. It is expected that the initial particle density will be lower and thus less rescattering should take place. In order to compensate for the reduced rescattering so that the freeze-out slope parameters agree with NA44, it is necessary to make $\beta_{\rm init}>0$ and thus reduce $T_{\rm init}$. In Fig. 13(c), $\tau_{\rm had}=10$ fm/c and so the initial particle density is expected to be correspondingly lower reducing even further the amount of rescattering and requiring even a higher value of $\beta_{\rm init}$ and lower value of $T_{\rm init}$ in order to agree with experiment. Figure 14, which shows the time evolution of the particle density for mid-rapidity particles ρ for the three different values of $\tau_{\rm had}$, verifies the above expectations for the dependence of the initial particle density on $\tau_{\rm had}$. The particle density is calculated by summing over all particles in the rapidity range $-1<y<1$ and dividing by the average volume determined from their space-time information. The time axis has the same meaning as in Fig. 13. It is seen that the particle densities are initially quite different for the different values of $\tau_{\rm had}$, although by the time of about 10 fm/c they begin to converge and then asymptotically approach the same value. For the $\tau_{\rm had}=1$ fm/c case, ρ is seen to be large ($\rho>1$ fm^{-3}) for times below about 2 fm/c. Although this raises the question of how valid the binary-scattering assumption is in this case for times less than 2 fm/c, it is probably still good enough to extract qualitative information about the early state. Figure 15 shows plots of $T_{\rm init}$, $\beta_{\rm init}$, and $\rho_{\rm init}$ (the initial particle density) versus $\tau_{\rm had}$ for calculations that all agree with the available measured singles observables, i.e., measured pion, kaon, and proton slope parameters, rapidity distributions, and multiplicities. Note that the quantities in Fig. 15 can be extracted directly from Figs. 13 and 14 at time=0. The initial state of the collision at hadronization is seen to depend strongly on $\tau_{\rm had}$. A small value of $\tau_{\rm had}$ results in large $T_{\rm init}$ and $\rho_{\rm init}$ and a small $\beta_{\rm init}$, whereas a large value of $\tau_{\rm had}$ results in smaller $T_{\rm init}$ and $\rho_{\rm init}$ and a large $\beta_{\rm init}$. Thus, the hadronic singles observables constrain the dependence of $T_{\rm init}$ and $\beta_{\rm init}$ on $\tau_{\rm had}$ but do not constrain $\tau_{\rm had}$ itself.

A possible way to constrain $\tau_{\rm had}$ using final-state hadrons is seen in Fig. 16. This figure shows the calculated $\tau_{\rm had}$ dependence of the pion source parameters determined from pion interferometry analyses of final-state midrapidity ($-1<y<1$) pion pairs from the present rescattering model. The transverse momentum cut for pions is $p_T<400$ MeV/c, the same as used for the calculation of Fig. 8. As seen, there is a relatively strong dependence of the radius parameters on $\tau_{\rm had}$, particularly for $R_{\rm long}$. Therefore, comparison of these calculated pion radius parameters with experimental pion interferometry results should allow $\tau_{\rm had}$ and thus the initial state of the collision at hadronization to be constrained. Figure 16 also shows a comparison of the calculated radius parameters for pion pairs with preliminary NA49 experimental results for Pb+Pb for the same average k_T and y range as used in the present calculations [10,11] as already shown in Fig. 10. As in Fig. 10, the dashed lines are simply projections of the experimental data points to allow for easy comparisons with the present calculations carried out for the different values of $\tau_{\rm had}$. The data clearly favor the $\tau_{\rm had}=1$ fm/c case over the others, and thus favor the initial parameter set of Table IV.

IV. PHYSICAL INTERPRETATION OF THE ''SIMPLE HADRONIZATION MODEL''

The ''simple hadronization model'' represented by Eqs. (1)–(4) and the parameter set of Table IV can be thought of conservatively as a simple parametrization of initial conditions for the present rescattering calculation that produces hadronic observables which qualitatively agree with experimental results. To what extent this parametrization describes the prerescattering state of the real system depends on the degree to which one can believe the rescattering calculation itself. If one takes the assumptions in the present rescattering calculation to be mostly valid, or, of equal importance, since it is found that the rescattering calculation itself is fairly insensitive to the details of the assumptions made, one could conclude that Eqs. (1)–(4) and Table IV qualitatively parametrize the prerescattering stage of CERN central Pb+Pb collisions.

Given this, the next step is to find the connection between this parametrization and a well-defined, more realistic hadronization model in order to extract a physical picture of the collision at this stage. As an example, the realistic hadronization model of Herrmann and Bertsch (HB) [13] will be used. The HB model is a thermal model that uses a string-inspired picture to describe the longitudinal direction of the hadronization. From the HB model, the coupled rapidity and m_T distribution at hadronization is

$$(1/m_T)d^2N/dm_T dy = K f_\eta(\eta) f_y(y-\eta, m_T), \qquad (10)$$

where

$$f_y(y-\eta,m_T) = m_T\cosh(y-\eta)/\{\exp[m_T\cosh(y-\eta)/T]\pm 1\}, \qquad (11)$$

$$f_\eta(\eta) = \exp[-\eta^2/2(\Delta\eta)^2], \qquad (12)$$

$$\eta = \tanh^{-1}(z_{\rm had}/t_{\rm had}), \qquad (13)$$

and where T is the kinetic temperature of the thermalized system, η is called the spatial rapidity, $\Delta\eta$ is the rms dispersion in η, $z_{\rm had}$ and $t_{\rm had}$ are the longitudinal position and time

of a particle at hadronization, $\pm$ refers to fermions (+) or bosons (−), and K is a constant. In the special case of hadronization of the system at an instantaneous proper time $\tau_{\rm had}$, as is the case for Eq. (4), it is seen from Eq. (13) that η becomes identical to y and in this case Eqs. (11) and (12) become

$$f_y(0,m_T)=m_T/\{\exp(m_T/T)\pm 1\} \tag{14}$$

and

$$f_\eta(y)=\exp[-y^2/2(\Delta\eta)^2]. \tag{15}$$

Note that a useful interpretation of $\tau_{\rm had}$ is that it is the lifetime of a ''prehadron'' in its own rest frame. Thus, one can imagine the prehadronization stage of the collision as a collection of ''prehadrons'' with lifetime $\tau_{\rm had}$ waiting to ''decay'' into hadrons, analogous to a collection of charged pions with mean lifetime 26 ns waiting to decay into muons. Comparing Eqs. (14) and (15) with Eqs. (1)–(3) above, and using the result from Table IV that $\beta_{\rm init}$ vanishes, it can be seen that the parameters $\sigma_{y\ \rm init}$ and $T_{\rm init}$ are related to $\Delta\eta$ and T of the HB model by

$$\sigma_{y\ \rm init}=\Delta\eta \tag{16}$$

and

$$T_{\rm init}\sim T. \tag{17}$$

A quantitative evaluation of the relationship between T and $T_{\rm init}$ can be made in the present case by ''fitting'' Eq. (1) to Eq. (14) for various particle types and requiring that $T_{\rm init}$ fits to 270 MeV (as in Table IV). It is found that T is bounded by values in the range of about 213 MeV (pions) to 235 MeV (nucleons) for particles used in the present calculation, such that

$$T=0.822T_{\rm init}\approx 222\pm 11\ \text{MeV}. \tag{18}$$

Note that the error bar in Eq. (18) is only reflecting the spread in T due to the influence of the different particle masses in the conversion from $T_{\rm init}$ to T.

Thus, it would be consistent with the HB hadronization model to conclude that under the assumption of hadronization at an instantaneous proper time, for CERN central Pb+Pb collisions the prehadronization stage of the collision has a short time duration, $\tau_{\rm had}=1$ fm/c, and this stage hadronizes with a finite initial rapidity spread $\sigma_{y\ \rm init}=1.2$, and at a high kinetic temperature $T\approx 222$ MeV. Other hadronization models could also be compared with the parametrization of Eqs. (1)–(4) and Table IV and could, in principle, give different physical interpretations.

In summary, a rescattering model including resonances coupled with a simple initial-state model has been used in an attempt to disentangle final-state rescattering to probe the early state in relativistic Pb+Pb collisions with measured hadronic observables. Although some general constraints on the initial-state model can be made using single-particle observables it is necessary, according to the present calculations, to couple this information with two-particle hadronic observables to uniquely determine the initial state.

ACKNOWLEDGMENTS

It is a pleasure to acknowledge Dave Hardtke, Gerd Welke, and Nu Xu for useful discussions relating to this work.

[1] B. Müller, Nucl. Phys. **A590**, 3c (1995); E. Laermann, *ibid.* **A610**, 1c (1996).
[2] H. Beker *et al.*, NA44 Collaboration, Phys. Rev. Lett. **74**, 3340 (1995).
[3] M. Gyulassy, S. K. Kauffmann, and L. W. Wilson, Phys. Rev. C **20**, 2267 (1979).
[4] H. Satz, Nucl. Phys. **A590**, 63c (1995); M. Gonin *et al.*, NA50 Collaboration, *ibid.* **A610**, 404c (1996).
[5] T. J. Humanic, Phys. Rev. C **53**, 901 (1996).
[6] J. Sullivan, M. Berenguer, B. V. Jacak, S. Pratt, M. Sarabura, J. Simon-Gillo, H. Sorge, and H. van Hecke, Phys. Rev. Lett. **70**, 3000 (1993).
[7] P. G. Jones *et al.*, NA49 Collaboration, Nucl. Phys. **A610**, 188c (1996).
[8] I. G. Bearden *et al.*, NA44 Collaboration, Phys. Rev. Lett. **78**, 2080 (1997).
[9] A. Franz *et al.*, NA44 Collaboration, Nucl. Phys. **A610**, 240c (1996).
[10] K. Kadija *et al.*, NA49 Collaboration, Nucl. Phys. **A610**, 248c (1996).
[11] H. Appelshäuser, Ph.D. thesis, University of Frankfurt, 1996.
[12] J. D. Bjorken, Phys. Rev. D **27**, 140 (1983).
[13] M. Herrmann and G. F. Bertsch, Phys. Rev. C **51**, 328 (1995).
[14] T. J. Humanic, Phys. Rev. C **50**, 2525 (1994).
[15] U. Goerlach *et al.*, HELIOS Collaboration, Nucl. Phys. **A544**, 109c (1992).
[16] M. Prakash, M. Prakash, R. Venugopalan, and G. Welke, Phys. Rep. **227**, 321 (1993).
[17] K. Hikasa *et al.*, Particle Particle Data Group, Phys. Rev. D **45**, 83 (1992).
[18] S. Pratt, Phys. Rev. D **33**, 1314 (1986); T. J. Humanic, Phys. Rev. C **34**, 191 (1986).
[19] S. Pratt, T. Csörgö, and J. Zimányi, Phys. Rev. C **42**, 2646 (1990).
[20] T. Csörgö, Phys. Lett. B **347**, 354 (1995); S. Chapman, P. Scotto, and U. Heinz, Phys. Rev. Lett. **74**, 4400 (1995).
[21] T. Csörgö and B. Lörstad, Nucl. Phys. **A590**, 468c (1995).